ELSEVIER

Journal of Power Sources 54 (1995) 501–507

JOURNAL OF POWER SOURCES

A new approach to the improvement of $Li_{1+x}V_3O_8$ performance in rechargeable lithium batteries

V. Manev [a], A. Momchilov [a], A. Nassalevska [a], G. Pistoia [b], M. Pasquali [c]

[a] *Central Laboratory of Electrochemical Power Sources, Bulgarian Academy of Sciences, Sofia 1113, Bulgaria*

[b] *Consiglio Nazionale delle Ricerche, Rome 00161, Italy*

[c] *Facolta di Ingegneria, Universita di Roma, Rome, Italy*

Abstract

A method for the improvement of the electrochemical properties of $Li_{1+x}V_3O_8$ is presented based on the partial modification of its crystal structure by the introduction of small amounts of inorganic compounds, such as H_2O, CO_2 and NH_3. The modification is performed by preliminary insertion of these molecules at high (H_2O) or ambient pressure (CO_2) or by use of appropriate method of synthesis (NH_3). A remarkable specific capacity of about 280 mAh/g has been achieved corresponding to the reversible intercalation of 3 equivalents of Li per mol $Li_{1+x}V_3O_8$. The high capacity performance and the good reversibility observed is assigned to the preliminary expansion of the interlayer spacing by the inorganic compounds inserted into it, this leading to an increased mobility and enhanced distribution of the Li^+ ions in the $Li_{1+x}V_3O_8$ layers.

Keywords: Rechargeable lithium batteries; Vanadium oxide

1. Introduction

A considerable number of vanadium oxides with a variable vanadium oxidation state were widely investigated in the last 15 years as perspective materials for rechargeable Li batteries. The largest specific energy can be obtained from the vanadium oxides where the transition metal is in its highest oxidation state, i.e. in its V^{5+} valency. Different modifications of V_2O_5 were studied, including the crystal forms of $Li_xV_2O_5$ such as α-$Li_xV_2O_5$ [1,2], β-$Li_xV_2O_5$ [3], ω-$Li_xV_2O_5$ [4,5], as well as the amorphous $Li_xV_2O_5$ [6,7] and $Li_xV_2O_5$ xerogel [8,9]. An alternative to obtain intercalation compounds with V^{5+} is the use of vanadates of transition [10] or alkali [10–17] metals.

From the last group the crystal $Li_{1+x}V_3O_8$ was the most intensively investigated and its good electrochemical performance in rechargeable Li cells was revealed in a series of papers [11–13]. It was shown recently that the amorphous form of this compound yields a larger specific capacity and a better reversibility than the crystal form [14]. A progress was achieved as well by the additions of SiO_2 and Al_2O_3 in the form of solid solution in $Li_{1+x}V_3O_8$ [15].

The present paper reveals an alternative method for the improvement of the electrochemical behaviour of the $Li_{1+x}V_3O_8$, associated with the partial modification of its crystal structure. This modification is achieved through the preliminary insertion of small amounts of some inorganic compounds into its layered structure and is expressed especially by the expansion of its interlayer spacing, which increases the specific capacity and the reversibility of the $Li_{1+x}V_3O_8$ cathodes.

2. Experimental

The starting crystal $Li_{1+x}V_3O_8$ was obtained as previously described [11,12] from a melt of V_2O_5 and Li_2CO_3 at 680 °C. The product was then ground in a ball mill to an average grain size of 1 μm. Then this powder was processed with H_2O in an autoclave or treated with CO_2 in an appropriate container.

The electrochemical tests were carried out with the aid of model electrodes, described in details in Ref. [18], in a three-electrode cell using 1 M $LiAsF_6$ in propylene carbonate (PC)–ethylene carbonate (EC) (1:2) as electrolyte. The electrodes were cycled at a constant-current density of 1 mA/cm^2, corresponding to a 3-h rate. V_2O_5 was obtained by thermal decomposition of NH_3VO_3 at 450 °C. The NH_3VO_3 and Li_2CO_3 were commercial products of Fluka. The X-ray dif-

SSDI 0378-7753(94)02135-P

fraction (XRD) analysis was carried out on a Philips APD 15 diffractometer with Cu Kα radiation. The specific surface area was evaluated by the BET method using a Strohlein & Co Area meter. The thermogravimetric analysis (TGA) was performed by a Perkin-Elmer TGS-2 analyser and differential thermal analysis (DTA) by a Perkin-Elmer DTA 1700 analyser.

3. Results and discussion

3.1. Effect of preliminary H_2O intercalation in the $Li_{1+x}V_3O_8$ crystal lattice

The crystal phase of $Li_{1+x}V_3O_8$ prepared by the classical high-temperature method [11,12] was subjected to forced intercalation of H_2O in an autoclave for 24 h at an elevated temperature. The XRD patterns of samples treated in the autoclave at different temperatures, shown in Fig. 1 reflect the structural alterations taking place during the forced intercalation of considerable amounts of H_2O in the $Li_{1+x}V_3O_8$ crystal phase. It can be seen that as the temperature of treatment increases the peak (100) corresponding to the lattice parameter a shifts to lower angles, which corresponds to a considerable increase in the interlayer spacing with respect to the starting phase. From this Figure one can also see that the interlayer spacing has several discrete values, and that the maximum one for $2\theta = 8.2°$ corresponds to $a = 11.3$ Å, which means that this lattice parameter becomes practically twice as large as that of the starting material ($a = 6.68$ Å).

The specific surface area of the samples treated in the autoclave at various temperatures (Fig. 2) shows unambiguously that along with the plastic deformations observed in the XRD patterns (Fig. 1) a considerable splitting of the crystallites takes place, resulting in an increase in the specific surface area of the material. The decrease in the specific surface area of the samples

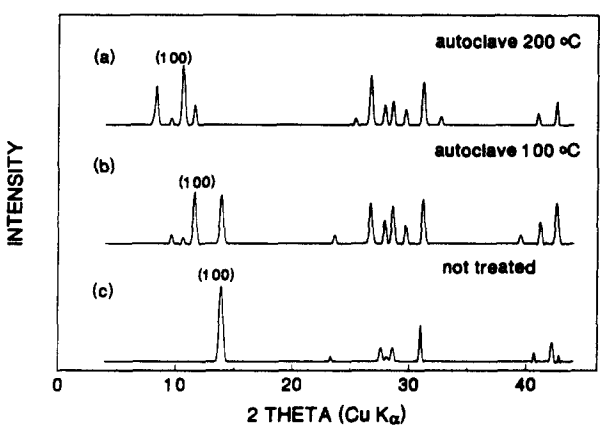

Fig. 1. Powder XRD patterns of autoclave-treated $Li_{1+x}V_3O_8$ at (a) 200 °C and (b) 100 °C compared with the pattern of a (c) not-treated one.

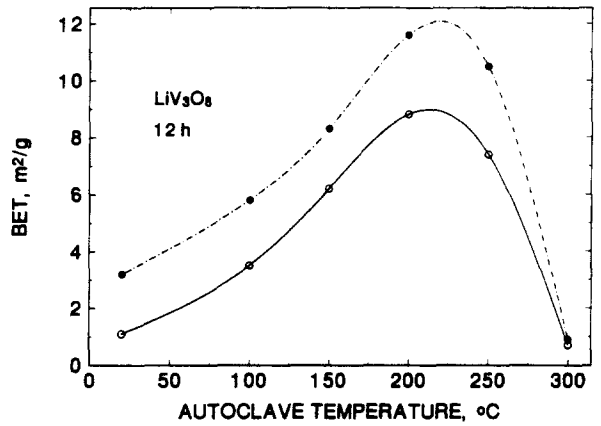

Fig. 2. Autoclave temperature vs. specific surface area of $Li_{1+x}V_3O_8$ with different initial specific surface areas: (○) 1.1 and (●) 3.2 m^2/g.

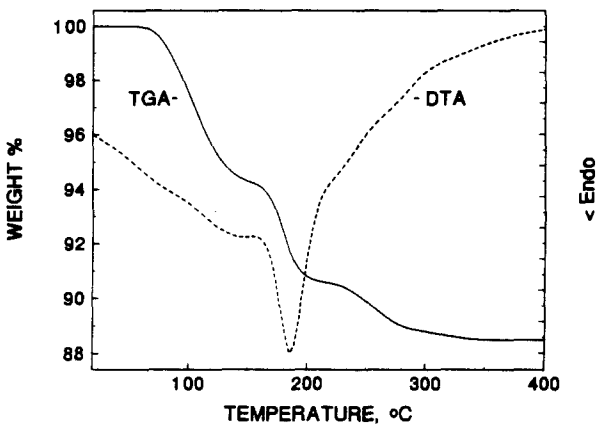

Fig. 3. TGA and DTA analyses of autoclave-treated $Li_{1+x}V_3O_8$ at 200 °C for 24 h.

treated in the autoclave above 250 °C (Fig. 2), probably reflects the beginning of a solid-state crystal growth.

The TGA curves of autoclave-treated $Li_{1+x}V_3O_8$ samples demonstrate (Fig. 3) that part of H_2O remains strongly bound in the $Li_{1+x}V_3O_8$ structure and can be completely removed at about 300 to 320 °C. TGA measurements also reveal that up to 8 molecules per mole of H_2O can be inserted in the elementary crystal lattice. The DTA analysis (Fig. 3) shows, in turn, that the elimination of H_2O is associated with a phase transition at temperatures around 180 °C.

From the XRD patterns of samples treated in autoclave at 200 °C and then dried for 12 h at different temperatures presented in Fig. 4(a) it can be concluded that the interlayer spacing of a part of the material remains considerably larger than that of the starting $Li_{1+x}V_3O_8$. Peaks of the (100) plane positioned at $2\theta = 9.6°$ and $2\theta = 11.7°$, corresponding to $a = 9.6$ Å and $a = 7.9$ Å, i.e. larger than that of the untreated material ($a = 6.68$ Å) can be observed even after a 24 h drying at 200 °C. It can be seen also that the samples dried at 250 °C (Fig. 4(b)) still preserve the peak positioned

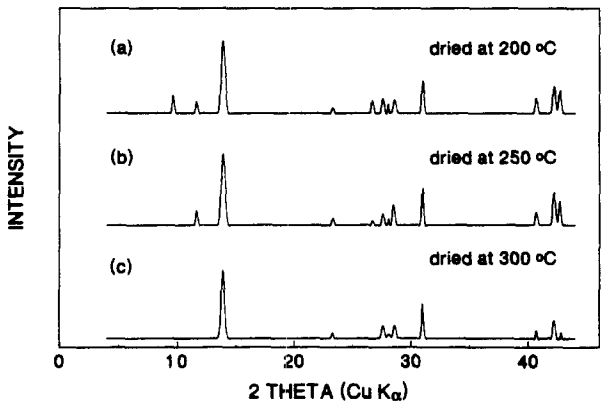

Fig. 4. Effect of drying temperature on the XRD patterns of the autoclave-treated $Li_{1+x}V_3O_8$.

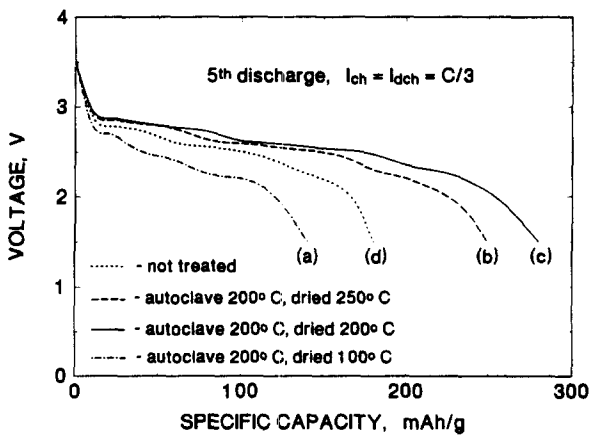

Fig. 5. Discharge curves of autoclave-treated $Li_{1+x}V_3O_8$ at 200 °C and then dried at 200 and 250 °C for 12 h.

at $2\theta = 11.7°$, corresponding to an interlayer spacing of $a = 7.9$ Å and that the drying at 300 °C leads to an XRD pattern equivalent to that of the starting compound (Fig. 4(c)).

The discharge curves at the 5th cycle of electrodes from samples treated in autoclave at 200 °C and then dried at 100 (Fig. 5(a)), 200 (Fig. 5(b)) and 250 °C (Fig. 5(c)), respectively, are compared with curves of the untreated material (Fig. 5(d)). It can be seen that the specific capacity of the autoclave-treated materials which are dried in the range from 200 to 250 °C is by 50% larger than that of the untreated, while the capacity of the samples dried at 100 °C is much lower than that of the starting material. This considerable positive effect of the remaining small amounts constitutional H_2O in $Li_{1+x}V_3O_8$ on its electrochemical behaviour could be explained with the increased interlayer spacing in the phase (Fig. 4), whereby the mobility and the uniform distribution of the Li^+ ions into the layer's structure are substantially enhanced. Obviously, the remaining considerable amounts of H_2O molecules after drying at 100 °C occupy the interlayer spacings in a manner that there are few sites left for the Li^+ ions, which has a negative effect on the specific capacity. However, by changing of the drying temperature the H_2O content in the structure can be controlled (Fig. 3) and the electrochemical properties thus optimized.

The cycling tests of electrodes from the autoclave-treated samples at 200 °C and then dried in the range from 200 to 250 °C (Fig. 6) reveal that the small amounts of the remaining structural H_2O in $Li_{1+x}V_3O_8$ (Fig. 3) improve not only the specific capacity but also its cycleability.

3.2. Effect of the insertion of CO_2 in $Li_{1+x}V_3O_8$ structure

A similar effect as that of H_2O can be observed with some other compounds, and one of these is CO_2. The prolonged treatment of $Li_{1+x}V_3O_8$ with CO_2 at room temperature, during several days at atmospheric pressure or several hours at 20 atmospheres substantially changes the XRD pattern of the material. Fig. 7 presents the powder XRD pattern of $Li_{1+x}V_3O_8$ processed at 1 atm CO_2 for 1 month compared with the one of the starting material. As can be seen from Fig. 7 in contrast

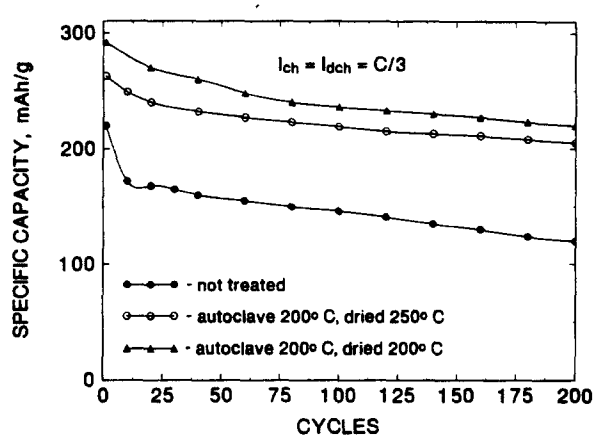

Fig. 6. Cycling tests of autoclave-treated $Li_{1+x}V_3O_8$ at 200 °C for 24 h and then dried at 200 and 250 °C.

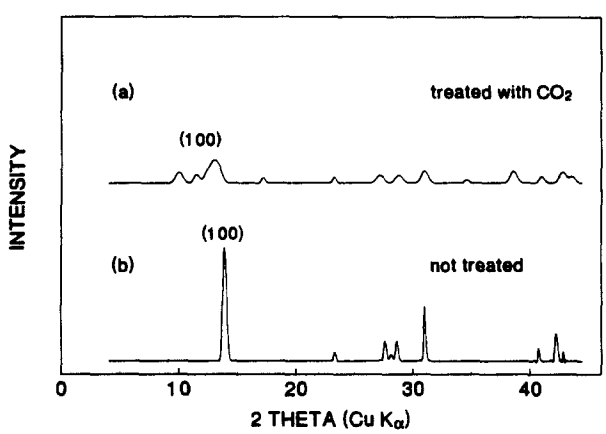

Fig. 7. XRD patterns of $Li_{1+x}V_3O_8$ treated with CO_2 at ambient temperature for (a) 1 month compared with a (b) not-treated one.

with the case of H_2O insertion considered above, the treatment with CO_2 leads to a flattening and broadening of the peaks, hence the material loses its crystallinity and obtains features of an amorphous phase. Simultaneously the strongly widened (100) peak shifts to lower angles, revealing an increase in the interlayer spacing, analogously with the H_2O-treated compounds (Fig. 1).

The TGA and DTA studies of $Li_{1+x}V_3O_8$ processed with 1 atm CO_2 for 1 month is shown in Fig. 8. In contrast with the results obtained with H_2O insertion, the TGA and DTA analyses shown that CO_2 evolves from the $Li_{1+x}V_3O_8$ structure at considerably lower temperatures up to 200 °C without any signs of a phase transition. The electrochemical behaviour of this material is also different from that of the untreated one. This is demonstrated in Fig. 9 where the differential capacity–potential plots of the $Li_{1+x}V_3O_8$ treated with CO_2 at ambient temperature for 1 month is compared with the same plot of the starting compounds. It can be seen that instead of two peaks, which are typical for $Li_{1+x}V_3O_8$ obtained from a melt, three very well-shaped discharge peaks appear in the plot of the CO_2-treated material. It is evident, as well, that a considerable increase in the specific capacity is obtained by the CO_2 treatment of the starting material and the calculation of the peaks area leads to the conclusion that each of them corresponds to 1 equivalent of Li per mol $Li_{1+x}V_3O_8$. It is worth noting that in spite of the fact that the XRD pattern tends to an amorphous phase (Fig. 7) the discharge curve (Fig. 10) exhibits the typical steps of the crystal $Li_{1+x}V_3O_8$ phase [11,12], corresponding to the peaks in Fig. 9, which distinguishes this material from the amorphous $Li_{1+x}V_3O_8$ obtained in water solution [14].

Fig. 11 illustrates the effect of cycling on the specific capacity of the CO_2-treated lithium vanadate. The comparison of Figs. 10 and 11 with the data in Figs. 5 and 6 reveals that the effect of traces of CO_2 in the $Li_{1+x}V_3O_8$ phase on the specific capacity of the latter is weaker than that of H_2O, but on the other hand its reversibility is better. These results naturally provoke

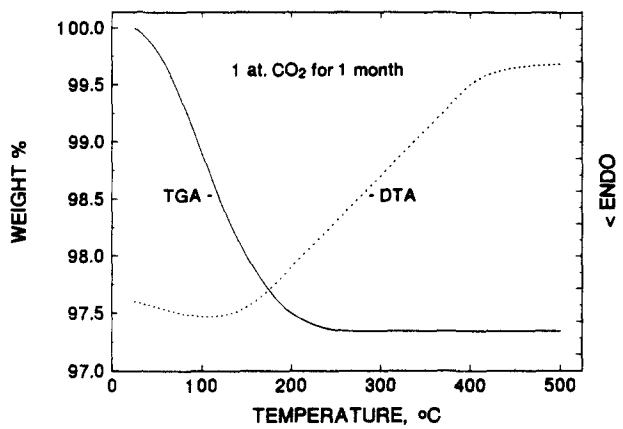

Fig. 8. TGA and DTA analyses of $Li_{1+x}V_3O_8$ treated with CO_2 at ambient temperature for 1 month.

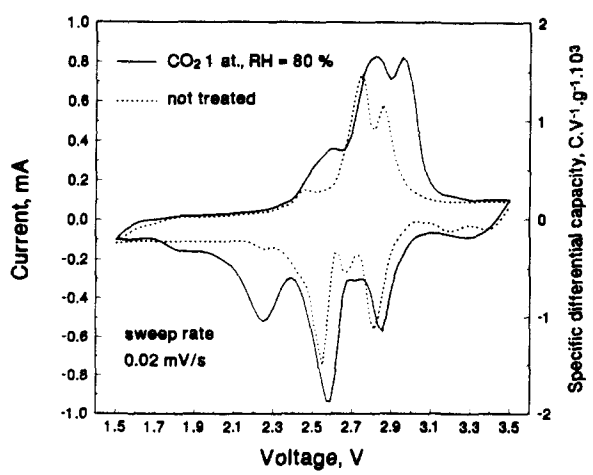

Fig. 9. Differential capacity–potential plots of the $Li_{1+x}V_3O_8$ treated with CO_2 at ambient temperature and r.h. = 80% for 1 month, compared with a not-treated one.

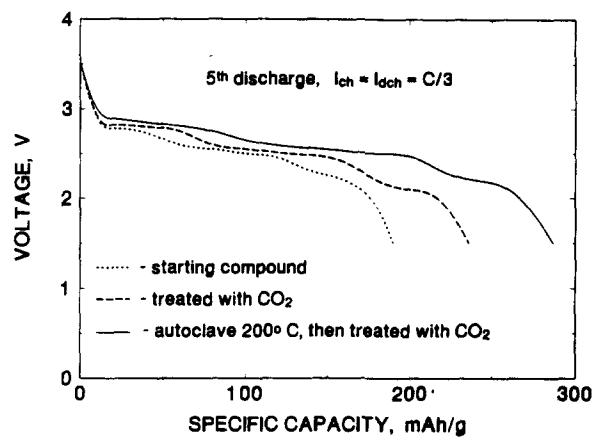

Fig. 10. Discharge curves of the starting $Li_{1+x}V_3O_8$ compared with that of a CO_2-treated one, and consecutively processed by H_2O and CO_2.

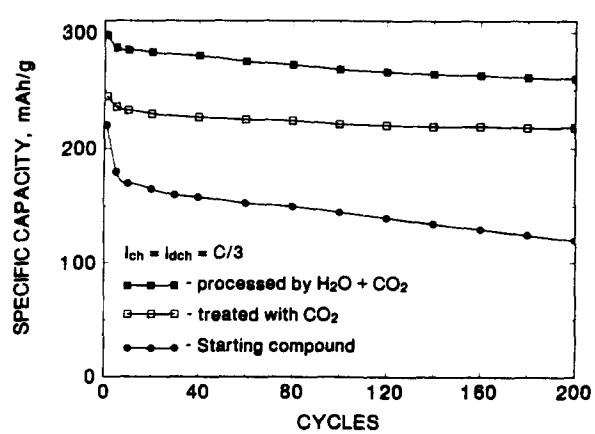

Fig. 11. Specific capacity vs. cycle number plots of the starting $Li_{1+x}V_3O_8$, CO_2-treated and consecutively processed with H_2O and CO_2.

the question: what will be the effect of the simultaneous treatment by H_2O and CO_2? The answer is presented in Figs. 10 and 11, showing the discharge curve and the cycleability at a 3-h charge/discharge rate of the sample successively treated with H_2O in an autoclave at 200 °C, then dried at 200 °C for 12 h and finally subjected to a prolonged treatment with CO_2 at room temperature. The specific capacity obtained of about 280 mAh/g is actually very attractive and corresponds to 3 Li equivalent per mole $Li_{1+x}V_3O_8$, which means that at the end of discharge, $Li_4V_3O_8$ is generated. In contrast with the results corresponding to the compound obtained from a melt [11,12] where only 2 equivalents of Li can be cycled and the assumption that the third step of the electrochemical reaction:

$$Li_3V_3O_8 + Li^+ - e^- \longrightarrow Li_4V_3O_8 \quad (1)$$

is not reversible, because it is associated with a substantial phase transition [14], the simultaneous treatment by H_2O and CO_2 leads to a product with a remarkable reversibility in the range $0<x<3$.

An explanation of the obvious advantages of the $Li_{1+x}V_3O_8$ samples processed by H_2O and CO_2 can be drawn from their XRD patterns presented in Fig. 12. It can be seen that in contrast with H_2O-treated $Li_{1+x}V_3O_8$, which has several discrete values of its interlayer spacing, the (H_2O+CO_2)-treated material preserves its crystallinity, but the peak of the (100) plane is splitted into three peaks, two of which are shifted to lower angles and are also wide and flat reflecting a large number of different interlayer spacings. A possible explanation of the results shown in Figs. 10 and 11 is that the considerable increase in the interlayer spacing determine the high specific capacity while the large scale of the different interlayer spacings, instead of discreate values (Fig. 1), leads to a more flexible structure which determines the good reversibility of this material.

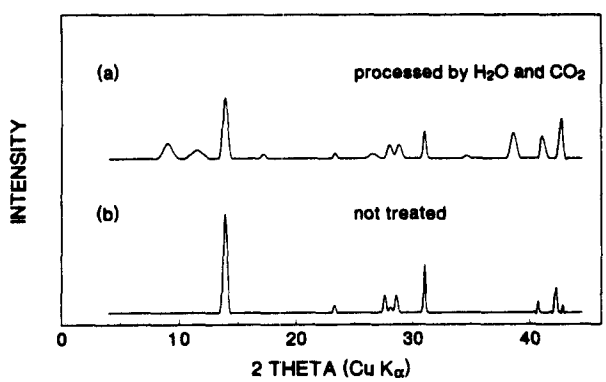

Fig. 12. Powder XRD patterns of (a) autoclave-treated $Li_{1+x}V_3O_8$ at 200 °C and after drying at 200 °C processed with CO_2 at ambient temperature for 15 days, and (b) non-treated $Li_{1+x}V_3O_8$.

3.3. Effect of NH_3 traces in the $Li_{1+x}V_3O_8$ structure

The crystal form of $Li_{1+x}V_3O_8$ can be prepared from NH_4VO_3 by performing two subsequent operations. First NH_4VO_3 is heated at 200 °C whereby $NH_4V_3O_8$ is obtained [19–21] according to reaction:

$$3NH_4VO_3 \longrightarrow NH_4V_3O_8 + 2NH_3 + H_2O \quad (2)$$

The product is then treated with a water solution of LiOH whereby the ion-exchange reaction occurs:

$$NH_4V_3O_8 + LiOH \longrightarrow LiV_3O_8 + NH_3 + H_2O \quad (3)$$

Fig. 13 shows a typical XRD pattern of $Li_{1+x}V_3O_8$ obtained by this method compared with that of a material synthesized from a V_2O_5–Li_2CO_3 melt [11,12]. As seen in Fig. 14, irrespectively that this material is obtained in a water solution it differs considerably from the amorphous material prepared by Pistoia et al. [14] since it has a well-expressed crystal structure. When a stoichiometric LiOH amount is used one can observe small foreign peaks, while in the case of a slight excess of LiOH the XRD pattern is similar to that obtained with the sample prepared by the high-temperature synthesis. There is only one substantial difference: instead of the

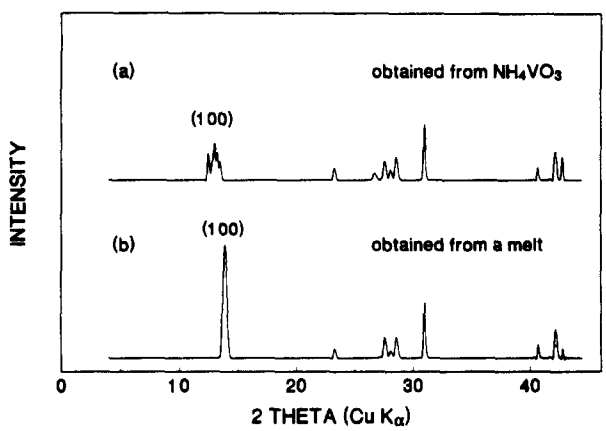

Fig. 13. Powder XRD patterns of $Li_{1+x}V_3O_8$ obtained from (a) NH_4VO_3 and (b) a melt.

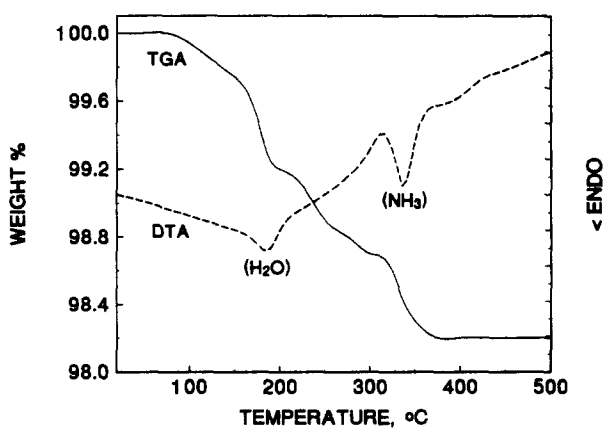

Fig. 14. TGA and DTA analyses of $Li_{1+x}V_3O_8$ obtained from NH_4VO_3.

regular peak of (100) at $2\theta = 14°$ with a maximum intensity there appears a group of peaks with smaller angles and lower intensities whose average value corresponds to about $2\theta = 13°$ (Fig. 11). This is a clear indication that using this method of $Li_{1+x}V_3O_8$ preparation, the product has a considerably larger interlayer spacing in comparison with the compound prepared from a melt.

TGA analysis (Fig. 14) and gas analysis during thermal treatment of the product revealed that a small amount of H_2O and NH_3 is present in the structure which can be eliminated at temperatures above 350 °C. DTA analysis (Fig. 14) indicates that the significant losses of H_2O and NH_3 are associated with phase transitions, which are observed at 180 and 320 °C, respectively.

The electrochemical performance of this $Li_{1+x}V_3O_8$, similarly to those containing H_2O and CO_2, exceeds that of the material obtained by the high-temperature synthesis. The discharge curve at a 3-h charge/discharge rate of $Li_{1+x}V_3O_8$ obtained by this method and then dried for 12 h at 200 °C is shown in Fig. 15. It is evident that the specific capacity obtained is comparable with those of the H_2O- and (H_2O+CO_2)-treated materials.

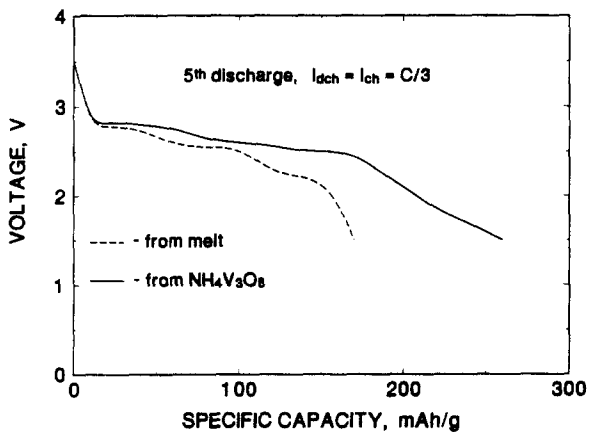

Fig. 15. Discharge curve of $Li_{1+x}V_3O_8$ prepared from (a) NH_4VO_3 compared with that (b) obtained by the classical high temperature method.

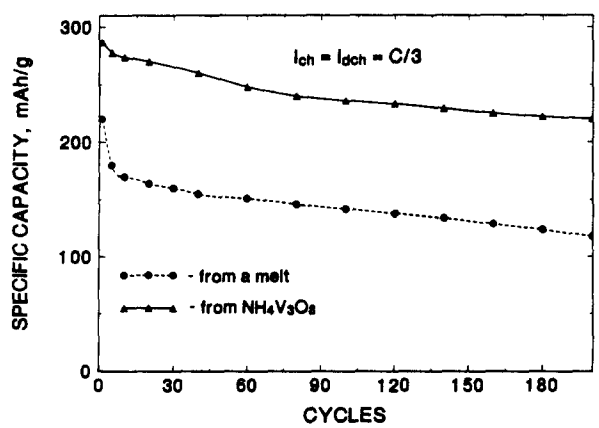

Fig. 16. Cell capacity vs. cycle number of $Li/Li_{1+x}V_3O_8(NH_3)$ button cells containing 1 M $LiAsF_6$ in ethylene carbonate–propylene carbonate (2:1) as electrolyte.

The long-term cycling tests at a 3-h rate of $Li_{1+x}V_3O_8$ prepared from $NH_4V_3O_8$ are illustrated in Fig. 16. It can be seen that $Li_{1+x}V_3O_8$ obtained by this method has a good reversibility which is however slightly lower than that of the (H_2O+CO_2)-treated material (Fig. 11). For a correct evaluation of this results it has to be emphasized that no efforts have been done so far for the optimization from this point of view.

4. Conclusions

Small amounts of some inorganic compounds such as H_2O, CO_2 and NH_3 can be integrated in the layered structure of LiV_3O_8. The elimination of CO_2 proceeds at comparatively lower temperatures (about 200 °C), while H_2O and NH_3 remain more strongly bound and can be eliminated at temperatures above 300 °C. Despite present in small amounts, these compounds substantially improve the electrochemical performance of the $Li_{1+x}V_3O_8$ electrode, increasing its specific capacity and enhancing its reversibility. The specific capacity obtained of about 280 mAh/g corresponds to a reversible exchange of 3 equivalent of Li per mole $Li_{1+x}V_3O_8$. This positive effect can be assigned to the expansion of the interlayer spacing, which leads to an increased mobility and enhanced distribution of the Li^+ ions between the layers. The best results are obtained by the simultaneous integration of H_2O and CO_2 in the $Li_{1+x}V_3O_8$ structure.

References

[1] D. Murphy, P. Christian, F. DiSalvo and J. Waszczak, *Inorg. Chem., 18* (1979) 2800.
[2] P. Dickens, S. French, A. Hight and M. Pye, *Mater. Res. Bull., 14* (1979) 1295.
[3] B. Zacho-Christiansen, K. West and T. Jacobsen, *Solid State Ionics, 9/10* (1983) 399–404.
[4] C. Delmas, S. Brethes and M. Menetrier, *J. Power Sources, 34* (1991) 113.
[5] Y. Sakurai, S. Okada, J. Yamaki and T. Okada, *J. Power Sources, 20* (1987) 173.
[6] M. Nabavi, C. Sanchez, F. Taulelle, J. Livage and A. Guibert, *Solid State Ionics, 28* (1988) 1183.
[7] K. West, B. Zachau-Christiansen, M. Ostergard and T. Jacobsen, *J. Power Sources, 20* (1987) 165.
[8] T. Miura, E. Sugiura, T. Kishi and T. Nagai, *Denki Kagaku, 56* (1988) 413.
[9] R. Baddour, J. Pereira-Ramos and R. Messina, *J. Electroanal. Chem., 277* (1990) 359.
[10] Y. Sukurai, H. Ohtsuka and J. Yamaki, *J. Electrochem. Soc., 135* (1988) 32.
[11] G. Pistoia, S. Panero, M. Tocci, R. Moshtev and V. Manev, *J. Solid State Ionics, 13* (1984) 12.
[12] G. Pistoia, M. Pasquali, M. Tocci, V. Manev and R. Moshtev, *J. Power Sources, 15* (1985) 13.

[13] V.L. Piccotto, K. Adendorff, D. Liles and M. Thackeray, *Solid State Ionics, 62* (1993) 297.
[14] G. Pistoia, M. Pasquali and G. Wang, *J. Electrochem. Soc., 137* (1990) 2365.
[15] T. Mijazaki, T. Ogino, Y. Masuda, H. Wada and T. Kawagoe, *US Patent No. 5 013 620* (7 May 1991).
[16] M. Pasquali and G. Pistoia, *Electrochim. Acta, 36* (1991) 1549.
[17] V. Manev, A. Momchilov, A. Nassalevska, G. Pistoia, M. Pasquali, *J. Power Sources, 43/44* (1993) 561.
[18] V. Manev, A. Momchilov, K. Tagawa and A. Kozawa, *Prog. Batteries Battery Mater., 12* (1993) 157.
[19] D. Wickham, *J. Inorg. Nucl. Chem., 27* (1965) 1939.
[20] T. Sas, V. Novojilov, J. Velicodni, V. Bulichev, V. Sorokin, *Neorg. Khim., 23* (1978) 3254.
[21] U. von Sacken and J. Dahn, *J. Power Sources, 26* (1989) 461.